catalysts

MDPI

Article

Numerical Study on Flow Channel Construction of Methanol Steam Reforming Reformer

Yujing Xiang, Huan Liu and Qi Zhang *

State key Laboratory of Green Chemical Engineering and Industrail Catalysis, School of Chemical Engineering, East China University of Science and Technology, Shanghai 200231, China; erjingxiang@163.com (Y.X.); liuhuan199710@163.com (H.L.)

* Correspondence: zhangqi@ecust.edu.cn; Tel.: +86-13601927588

Abstract: Compared with the traditional granular catalyst, a mesh-type structured CuZn-based catalyst prepared by the self-growth ordered nanoporous carrier γ-Al_2O_3/Al can adapt to the MSR reaction system with high flux, strong mass transfer and heat transfer, and can promote the practical process. In this study, the kinetic experiment using a CuZn-based structured catalyst was carried out, and a nonlinear single-rate PL model was established. Based on this, a 3D theoretical model of the MSR reformer was drawn in COMSOL Multiphysics. By changing the stacking form and mesh shape of the catalyst to construct the flow channel, the chemical reaction process, heat transfer process, and mass transfer process of the CuZn structured catalyst in the reformer under different flow channels are further simulated, which provides a theoretical basis for studying the enhancement of the MSR reaction and the development of a supporting micro hydrogen production system.

Keywords: methanol steam reforming; CuZn-based structured catalyst; electrodeposition intrinsic kinetics; flow channel construction

check for updates

Citation: Xiang, Y.; Liu, H.; Zhang, Q. Numerical Study on Flow Channel Construction of Methanol Steam Reforming Reformer. *Catalysts* **2024**, *14*, 913. https://doi.org/10.3390/catal14120913

Academic Editor: Concetta Ruocco

Received: 9 November 2024
Revised: 3 December 2024
Accepted: 6 December 2024
Published: 11 December 2024

Copyright: © 2024 by the authors. Licensee MDPI, Basel, Switzerland. This article is an open access article distributed under the terms and conditions of the Creative Commons Attribution (CC BY) license (https://creativecommons.org/licenses/by/4.0/).

1. Introduction

Amid the dual crises of energy and environment, hydrogen energy has emerged as a focal point of research for various countries [1,2]. With the technological advancement of proton-membrane fuel cells (PMEFCs), the challenges in hydrogen energy development have shifted from utilization to transportation and storage [3–5]. Compared to the most commonly used high-pressure gaseous hydrogen transportation technology, methanol hydrogen storage technology stands out due to its high hydrogen storage density, a carbon-to-hydrogen ratio of 1:4, and its low sulfur content, making it a preferred feedstock for steam reforming hydrogen production. Utilized in distributed online hydrogen generation, it can effectively address the issues of hydrogen storage and transportation, thereby reducing the costs associated with hydrogen energy logistics. The development of fast-startup, high-efficiency micro hydrogen production systems has become a significant research focus, with the coupling of catalysts and reformer being a key technology in such systems.

The main reaction of methanol reforming for hydrogen production is shown in Formula (1), and the side reactions include methanol decomposition and reverse water gas shift reaction (rWGS), shown in Formulas (2) and (3):

$$CH_3OH + H_2O \rightarrow 3H_2 + CO_2 \quad \Delta H^0 = +49.4\ \text{kJ/mol} \tag{1}$$

$$CH_3OH \rightarrow 2H_2 + CO \quad \Delta H^0 = +92.0\ \text{kJ/mol} \tag{2}$$

$$CO_2 + H_2 \rightarrow H_2O + CO \quad \Delta H^0 = +41.4\ \text{kJ/mol} \tag{3}$$

Some possible side reactions include methanation, formaldehyde synthesis, dehydrogenation, dehydration, etc., shown in Formulas (4)–(7):

$$2CH_3OH \rightarrow CH_3 + CO_2 + 2H_2 \quad \Delta H^0 = -66.9\ \text{kJ/mol} \tag{4}$$

$$CH_3OH \rightarrow CH_2O + H_2 \qquad \Delta H^0 = +84.7\ \text{kJ/mol} \tag{5}$$

$$2CH_3OH \rightarrow HCO_2CH_3 + 2H_2 \qquad \Delta H^0 = +64.4\ \text{kJ/mol} \tag{6}$$

$$2CH_3OH \rightarrow (CH_3)_2O + 2H_2O \qquad \Delta H^0 = -23\ \text{kJ/mol} \tag{7}$$

With the traditional granular catalyst, it is difficult to realize regular stacking, and it easily leads to uneven temperature and concentration distribution in the reformer; it also has the disadvantages of large pressure drop, easy blockage and wear, and low efficiency, which make it difficult to be adapted to the requirements of the reaction system with high flux and strong mass and heat transfer [6]. About the design of the channel structure, few studies are using the structural characteristics of the catalyst itself to build the flow channel and study the chemical reaction process and how mass transfer and heat transfer of the system are developed, most studies change the internal structure of the reactor to adjust the flow channel [7,8].

In the previous work of this study, by constructing Cu_2O/ZnO synergistic catalytic sites, we developed a mesh-type structured CuZn /γ-Al_2O_3 catalyst with high temperature resistance, long life, fast start-up, and high activity [9]. On this basis, the kinetic behavior of a CuZn-based core-shell catalyst was carried out. Only the MSR reaction was considered, and the power-law single-rate equation was used to describe the reaction kinetic process. Furthermore, the kinetic parameters were applied to the reformer, and the effects of the catalyst distribution configuration and mesh shape on the chemical reaction process and mass and heat transfer process of the MSR reaction were studied, which provided a theoretical basis for the study of strengthening the MSR reaction and the development of a supporting micro hydrogen production system.

2. Results and Discussion

2.1. Catalyst Distribution Enhances the MSR Reaction Process

The simulation results in the micro-reformer show that the conversion rate Model C (97.32%) > Model B (96.12%) > Model A (95.22%), which is consistent with the experimental results and the literature results [10,11], as shown in Figure 1. This may be related to the effect of different catalyst distributions on fluid disturbance.

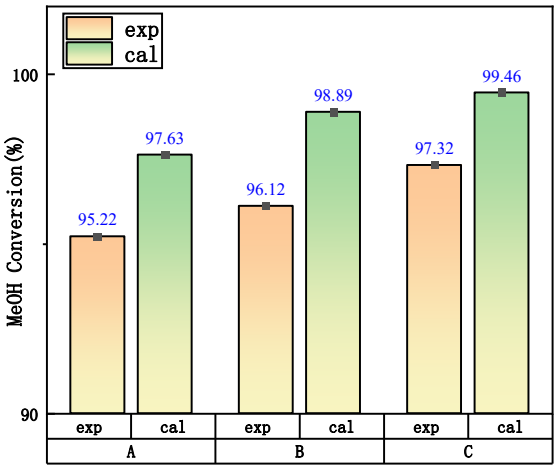


Figure 1. Simulated and experimental values of methanol conversion at 275 °C for different catalyst distribution configurations.

As shown in Figure 2a–c, the hydrogen concentration at the inlet is Model C > Model B > Model A. This is because the effective fluid contact area of the catalyst at the inlet increases, which increases the flow resistance, increases the residence time of the reactants, and promotes the reaction. From the streamline distribution, Figure 2d–f, the streamline of Model A is mainly concentrated in the middle of the reformer, and there are few reactants passing on both sides, which greatly reduces the utilization rate of the reformer as a whole.

The streamline of Model B is mainly concentrated on both sides of the reactor, and less in the middle. In contrast, the streamlines of Model C are denser on both sides and in the middle of the reactor; that is, the reactor utilization rate is Model C > Model B > Model A, which explains the reason for the higher conversion rate of Model C.

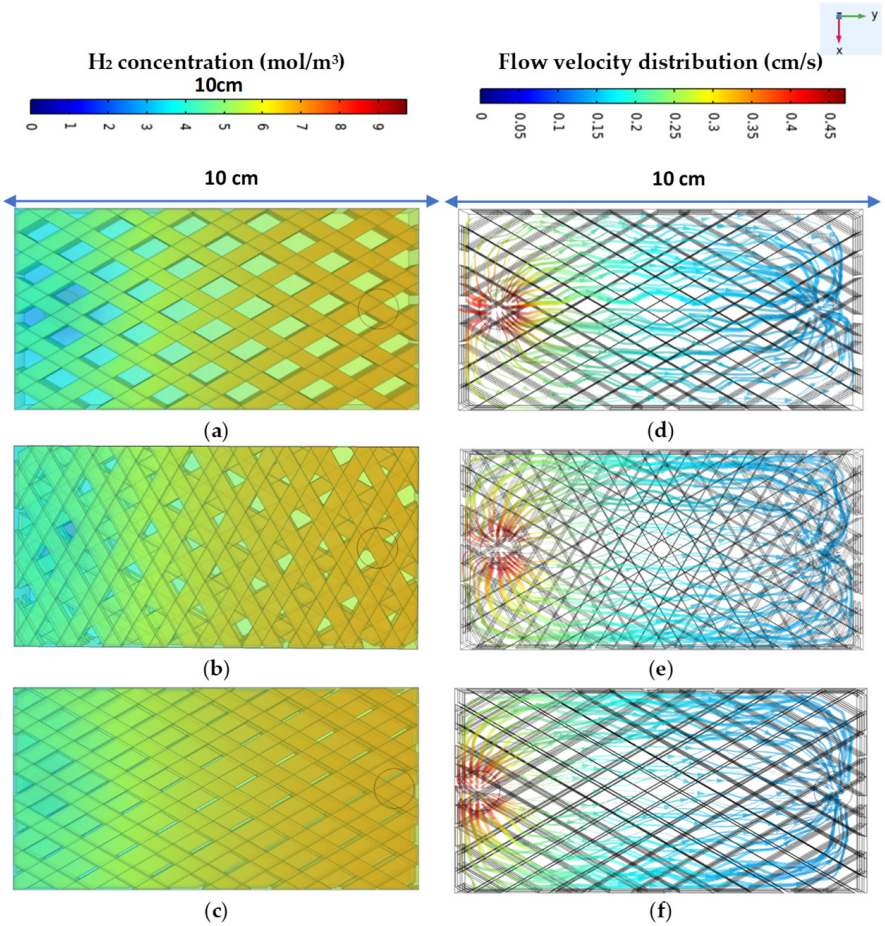


Figure 2. H_2 concentration distribution in microreactor: (**a**) Model A, (**b**) Model B, (**c**) Model C. Flow velocity distribution in microreactor: (**d**) Model A, (**e**) Model B, (**f**) Model C.

The concentration distribution of the reactant methanol in the reformer is shown in Figure 3a–c. The horizontal line effect of the turbulence [12] can be further analyzed. The concentration distribution is Model C > Model B > Model A at the lower right of the reactor, which is due to the turbulence effect of the catalyst on the fluid. The Model A fluid flows directly through the channel from the inlet to the outlet, resulting in a dead zone at the lower right. The effective contact area between the Model C catalyst and the fluid is larger, and the fluid collides with the catalyst. Lateral diffusion reduces the dead zone [13] and improves the utilization rate of the reformer.

The streamlines at the entrance are shown in Figure 3c–e. Compared with Model A and Model B, the streamline distribution density around the entrance of Model C is greater than that at the center, which confirms that the turbulence will exert a transverse diffusion force on the fluid. The above shows that the mass transfer efficiency of Model C is the best.

Further analysis of the heat transfer situation, as shown in Figure 4a, is the temperature distribution along the vertical direction (z-axis direction) at the entrance, exit, and geometric center of the reactor at the entrance of the mesh alignment in Model A and the optimal mass transfer efficiency of Model C. The temperature distribution of Model A is the inverted 'M' type. The temperature near the boundary of the reformer is high, and the change trend along the longitudinal direction is large. The temperature in the middle area of z = 0.1~0.3 is low, and the temperature difference is not large, which is related to the

streamline of Model A being mainly concentrated in the middle, as shown in Figure 2d. The temperature distribution along the axial direction at the inlet and outlet of Model C is basically unchanged along the z-axis direction. Only in the small dead zone formed, as shown in Figure 3c the temperature changes greatly, which is related to the uniformity of the Model C streamline on both sides and in the middle, as shown in Figure 2f. At the same time, from the temperature difference of the same transverse section of the inlet–geometry center–outlet, it can be seen that the three curves of Model C are almost overlapped, and the temperature difference is about 0.1 °C. However, the curves of Model A are almost overlapped, and the temperature decreases along the transverse line (y-axis direction). The temperature distribution of the geometric center of the reactor along the transverse line shown in Figure 4b is consistent with it. This shows that the heat transfer in the longitudinal and transverse directions can be promoted by constructing a suitable flow channel to form a certain disturbance.

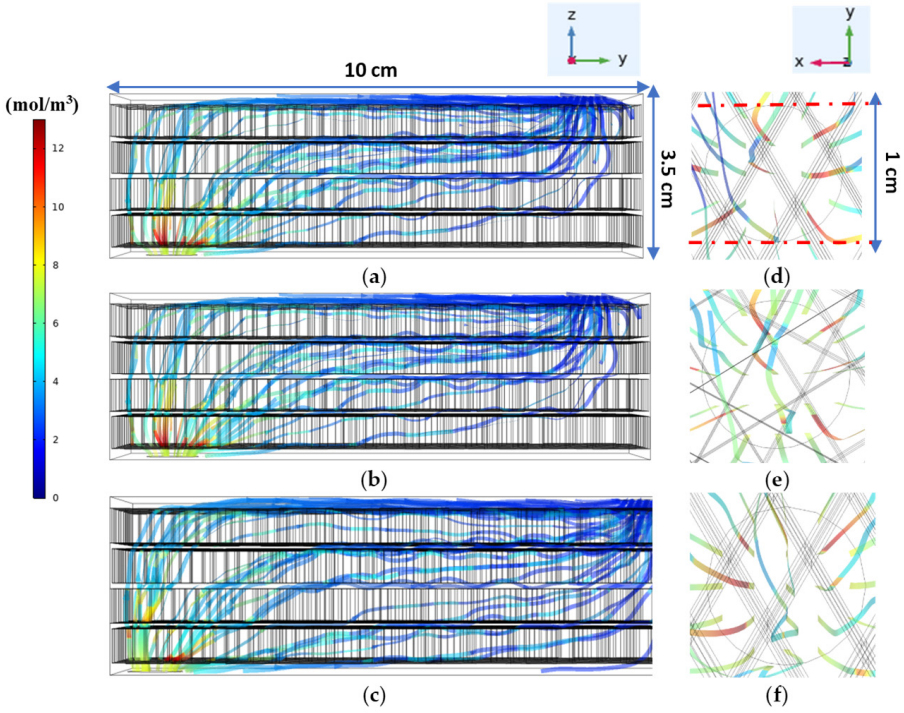


Figure 3. Methanol concentration distribution in microreactor: (**a**) Model A, (**b**) Model B, (**c**) Model C. Methanol concentration distribution at inlet: (**d**) Model A, (**e**) Model B, (**f**) Model C.

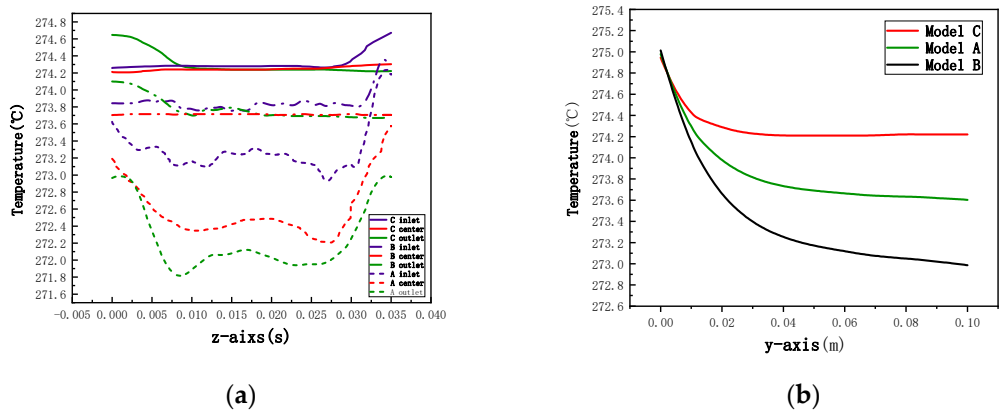


Figure 4. (**a**) The temperature distribution along the vertical direction (z-axis direction) at the inlet, outlet and geometric center of the reactor with different models, (**b**) The temperature distribution of the geometric center of the reactor along the y-axis of different models.

2.2. The Channel Shape of the Catalyst Enhances the MSR Reaction Process

The simulation results of the methanol conversion rate with different channel shapes are circular (99.11%) > square (98.35%) > equilateral triangle (98.12%) > rhombus (97.63%), which is the same as the order of equivalent diameter. That is, in the case of the same catalyst volume, the order of the catalyst surface area is opposite to that of the equivalent diameter, but the difference is small. In this case, the deviation of the flow channel shape from the fluid affects the concentration distribution, and the influence of the shape on the heat and mass transfer inside the catalyst channel is the main factor causing different conversion rates.

Under the same catalyst distribution, Model A, the deviation of methanol streamline in the reformer with different pore shapes is shown in Figure 5. The deviation of the channel to the streamline is rhombus > triangle > square > circle, which may be related to the collision angle between the fluid and the channel. The larger the collision angle between the fluid and the channel, the higher the final deviation. Appropriate deviation contributes to the uniform distribution of concentration. Excessive deviation causes the fluid to concentrate on both sides of the reactor, which reduces the utilization efficiency of the reactor. At the same time, the average diffusion distance between the pores is rhombus > equilateral triangle > square > circle. The shorter the diffusion path, the smaller the diffusion resistance and the more conducive to strengthening the reaction. Finally, it is determined that the conversion rate of circular pores is the highest.

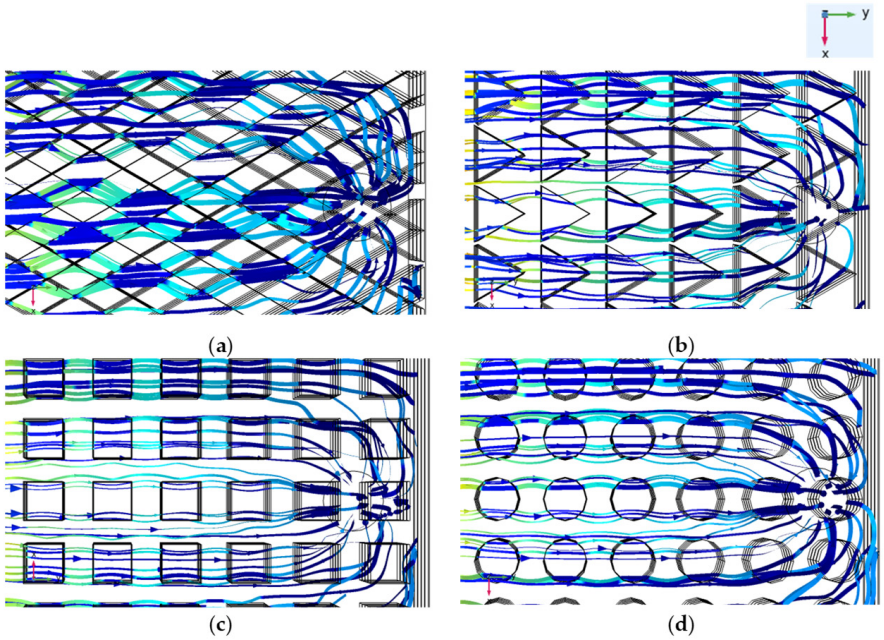


Figure 5. Effects of channel shapes on methanol concentration distribution: (**a**) Rhombus, (**b**) Equilateral triangle, (**c**) Square, (**d**) Circle.

The simulation results of pressure drop in the micro-reformer with different channel shapes are circular (0.059 Pa) < square (0.064 Pa) < equilateral triangle (0.071 Pa) < rhombus (0.076 Pa). According to the calculation formula of pressure drop ΔP, Formula (8), it can be seen that the pressure drop ΔP is inversely proportional to the equivalent diameter under the same channel friction factor, channel length, fluid flow rate, and fluid density, which is consistent with the simulation results. The larger the equivalent diameter, the smaller the pressure drop, and the validity of the simulation results is also verified.

$$\Delta P = \frac{2f\rho v^2 \Delta L}{d_e} \tag{8}$$

Here, f is the friction factor of the channel, the same fixed value under the same channel material; ρ is the fluid density; v is the fluid flow rate; L is the channel length; and d_e is the equivalent diameter.

The radial effective thermal conductivity λ_{er} can measure the heat transfer behavior of the mesh-type structured catalyst in the radial direction [14,15]. The radial effective thermal conductivity λ_{er} is shown in Formula (9):

$$\lambda_{er} = \lambda_g[a + b(\mathrm{RePr})] \tag{9}$$

$$\mathrm{Re} = \frac{\rho d_e v}{\mu} \tag{10}$$

$$\mathrm{Pr} = \frac{C_p \mu}{\lambda} \tag{11}$$

λ_g is the gas phase thermal conductivity, a and b are constants, Re is the Reynolds number, Pr is the Prandtl number, μ is the fluid viscosity, C_p is the specific heat capacity of the fluid at constant pressure, and λ is the thermal conductivity. The term a represents the static heat conduction capacity, and $b(RePr)$ represents the convective heat transfer capacity. When other conditions are the same, λ_{er} is positively correlated with de, so the radial effective thermal conductivity is round > square > triangle > rhombus; that is, the circular catalyst has better heat transfer capacity in the longitudinal direction, which is conducive to accelerating the heat transfer inside the catalyst, reducing the temperature difference between the inside and outside of the catalyst and the uneven temperature distribution of the bed, improving the utilization rate of the catalyst and the catalytic activity. In this study, the reaction condition is T = 548.15 K, p = 1 atm. When the mixed fluid passes through the catalyst bed, the velocity is 0.2 m/s, the volume ratio of the mixed fluid is $V_{H_2O} : V_{MeOH} : V_{N_2} = 2 : 1 : 3$; then, we can obtain the dynamic viscosity and density of the mixed fluid, $\mu = 1.755 \times 10^{-4}$Pa/s, $\rho = 0.539$kg/m^3. The circular channel has the largest $d_e = 0.700$, so we can obtain $R_e \approx 430 < 2000$, which belongs to the laminar flow and is consistent with the simulation conditions.

There is a certain functional relationship between Sh and Re and Sc [16], shown in Formula (12):

$$Sh = \frac{k d_e}{D_{AB}} = f(\mathrm{Re}, Sc) \tag{12}$$

k is the mass transfer coefficient, D_{AB} is the diffusion coefficient, and Sh is positively correlated with de. The Sh value, circular > square > triangle > rhombus, represents the ability of fluid mass transfer. The larger the Sherwood number, the stronger the fluid mass transfer, the smaller the concentration difference between the inner and outer surfaces of the catalyst, and the higher the utilization rate of the internal active components of the catalyst, thereby improving the catalytic activity.

In order to reflect the flow in the micro-reformer, the fluid flow particle tracking module of transient research was used to collect the fluid residence time distribution as shown in Figure 6, and the average residence time and dimensionless variance of the fluid were calculated. The results are shown in Table 1. For various catalyst channel types, the degree of backmixing was square > circular > regular triangle > rhombus, and the average residence time was triangle > square > round > rhombus. Due to the disturbance of the catalytic bed to the fluid, the dimensionless variance of the fluid is greater than 0 but around 0.1, which means that there is a certain degree of backmixing but still close to the plug flow, and it promotes the mixing of the reactants. At the same time, the residence time is increased. Prolonging the residence time is beneficial to increase the contact time between the reactants and the catalyst and promote the conversion of the reactants, but too long a residence time will reduce the reaction rate.

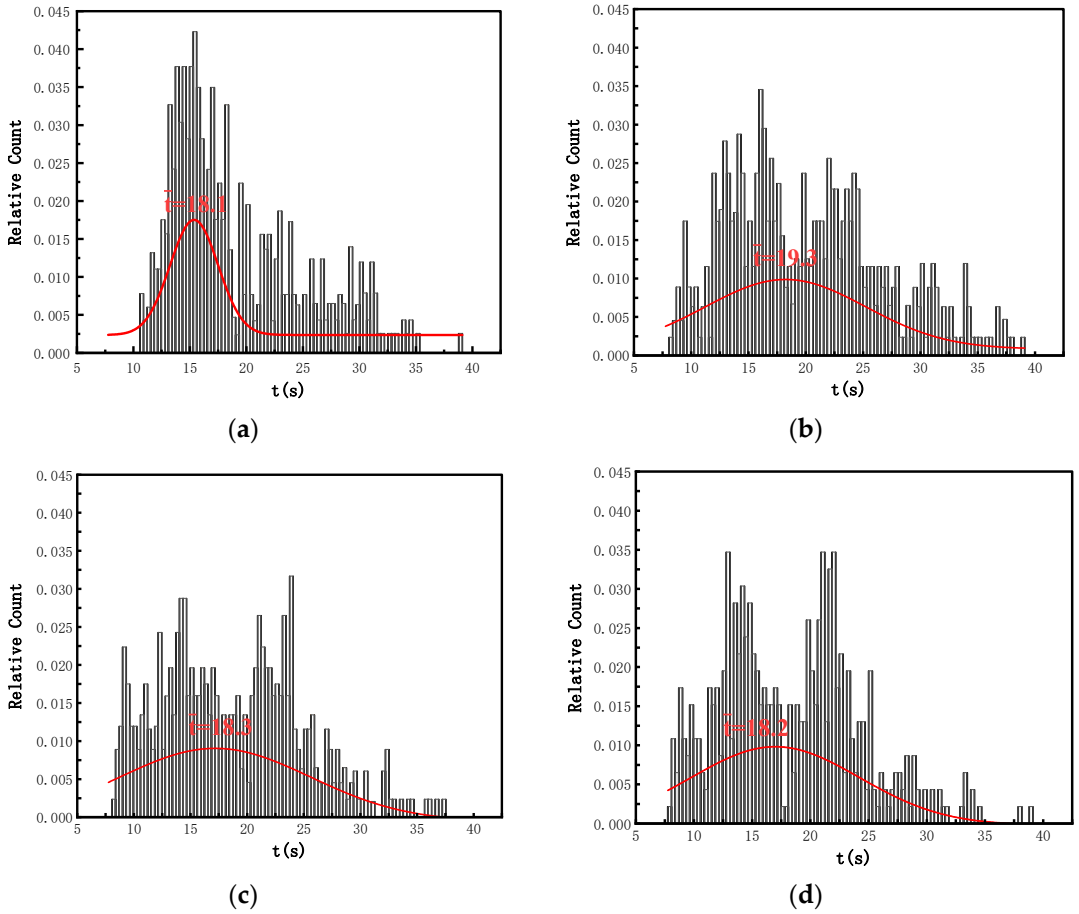


Figure 6. Effects of channel shapes on residence time distribution: (**a**) Rhombus, (**b**) Equilateral triangle, (**c**) Square, (**d**) Circle.

Table 1. Residence time in the microreactors with different channel shapes.

	Rhombus	Equilateral Triangle	Square	Circle
Mean residence time $\bar{t}$ (s)	18.1	19.3	18.3	18.2
Dimensionless variance σ_θ^2	0.0867	0.1034	0.1059	0.1045

3. Model Development

3.1. Reformer Design

The monolithic structured catalyst has parallel channels arranged in a row and has a uniform and regular structure. It is stacked to form a catalyst bed in the reformer. Compared with the traditional granular catalyst, it can avoid the wear caused by particle movement. At the same time, it has an open structure, low pressure drop, and short diffusion path, and it improves the selectivity and catalytic efficiency of the reaction [17–19]. Different catalyst distribution configurations and mesh shapes can construct different flow channels, resulting in different flow fields and temperature distributions, which in turn affects the utilization rate of the catalyst.

According to the structural parameters given in Table 2, the geometric structure of the mesh-type structured catalyst in the reformer was established [20,21]. The overall structure of the reformer is shown in Figure 7a,b.

Table 2. Structural parameters of the micro-reformer.

Item	Parameter
Diagonal length of rhomboid channel (mm)	1.225 × 0.629
Catalyst length × width × thickness (cm)	10 × 5 × 0.06
Number of catalyst layers	45
Gap between two layers of catalyst (cm)	0.01
Gap between catalyst and plate (cm)	0.18
Reactor length × width × height (cm)	10 × 5 × 3.5
Inlet and outlet radius (cm)	0.5
Reactant	$CH_3OH + H_2O$
Product	$CH_3OH + H_2O + CO_2 + H_2 + CO$
Fluid velocity(m/s)	0.02
Feed temperature (K)	548.15
Reformer temperature (K)	548.15
Mole fraction: water/methanol	2/1
Pressure (atm)	1
Structured catalyst: ($Cu_{9.6}Zn_{1.5}/\gamma$-Al_2O_3/Al)	
Catalyst porosity: ε_p	0.4
Catalyst effective thermal conductivity: k_s(W/(m × K))	3
Catalyst tortuosity: τ_p	1

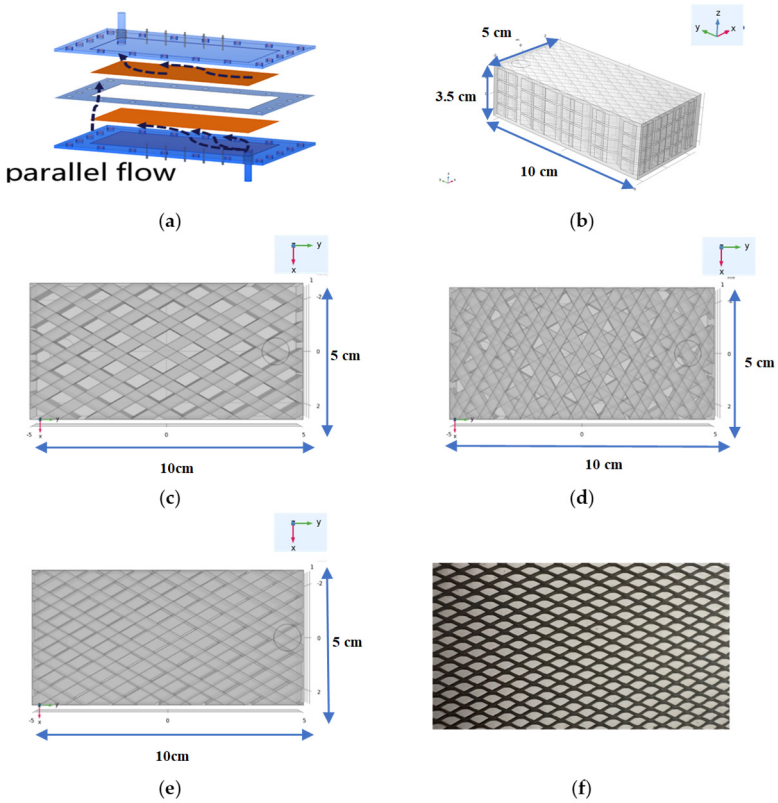
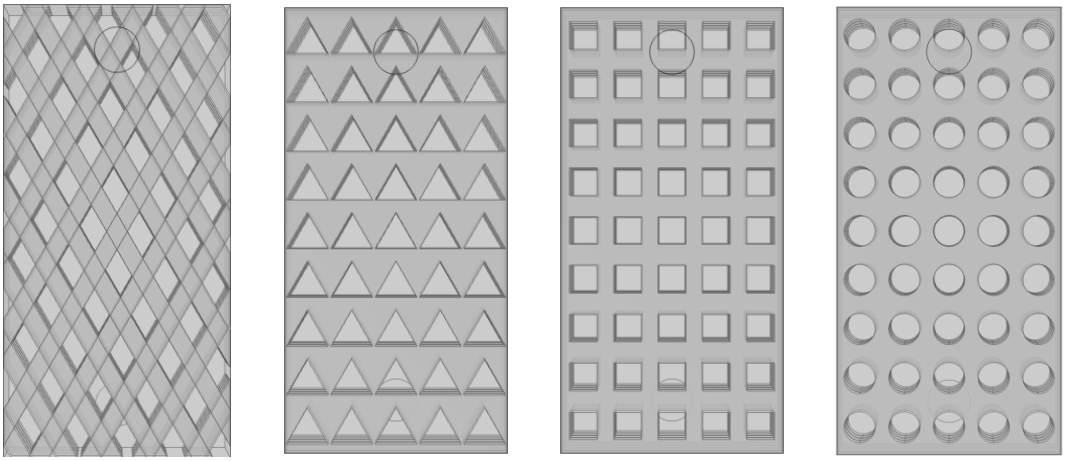


Figure 7. The geometry of the reforming reformer: (**a**) schematic, (**b**) overall structure, (**c**) Model A, (**d**) Model B, (**e**) Model C, (**f**) single-layer mesh-type catalyst physical diagram.

Three different catalyst distribution forms were designed, as shown in Figure 7c–e. The actual morphology of the single-layer catalyst is shown in Figure 7f. The meshes of the layers of catalyst in Model A are aligned. The catalyst of each layer in Model B is rotated at a certain angle compared with the previous layer, and the edges of each layer of catalyst in Model C are opposite to the mesh of the next layer. From Model A to Model C, the overlap area of the adjacent two-layer grids increases in turn.

Based on the study of the different catalyst distribution configurations, the effects of different mesh shapes on the reaction were further simulated [22]. Using the Model A configuration, as shown in Figure 8, four common mesh shapes were selected: rhombus, triangular, square, and circular. Table 3 shows the structural parameters of the four mesh shapes. The channel height and channel area of the four shapes are equal to ensure that the catalyst dosage, channel number, and bed porosity are the same under the same catalyst volume. The overall methanol conversion rate was investigated, and the transfer characteristics of the channels were studied, including the effects of momentum transfer, heat transfer, and mass transfer, which have a certain influence on the activity of the catalyst.



(**a**) (**b**) (**c**) (**d**)

Figure 8. Different channel shapes of catalysts: (**a**) Rhombus, (**b**) Equilateral triangle, (**c**) Square, (**d**) Circle.

Table 3. Structural parameters of catalyst channels.

Parameter	Rhombus	Equilateral Triangle	Square	Circle
Channel area (mm^2)	0.385	0.385	0.385	0.385
Equivalent diameter (mm)	0.415	0.544	0.620	0.700
Perimeter (mm)	3.708	2.829	2.482	2.200
Height (mm)	0.6	0.6	0.6	0.6
Surface area per layer (mm^2)	85.72	85.20	84.99	84.82

3.2. Kinetic

In the previous work, the optimal reaction conditions were optimized by thermodynamic analysis, and the life of the CuZn catalyst in the reformer was tested. The methanol conversion rate with time at the highest reaction temperature of 548.15 K is shown in Figure 9. The initial conversion decreased slightly, and the conversion rate tended to be stable at about 90% within 3–26 h. Therefore, the subsequent intrinsic kinetic experiments were carried out within 3–26 h to ensure the accuracy of the experimental data.

Under the premise of catalyst stability and elimination of internal and external diffusion effects, 25 sets of intrinsic kinetic experiments of the methanol steam reforming reaction were investigated in this experiment, and 16 sets were selected as model data. The reaction conditions were as follows: pressure of 1 atm, water/alcohol ratio of 2/1, temperature of 498.15–548.15 K, W/F of 32.2–51.7 kg·s/mol.

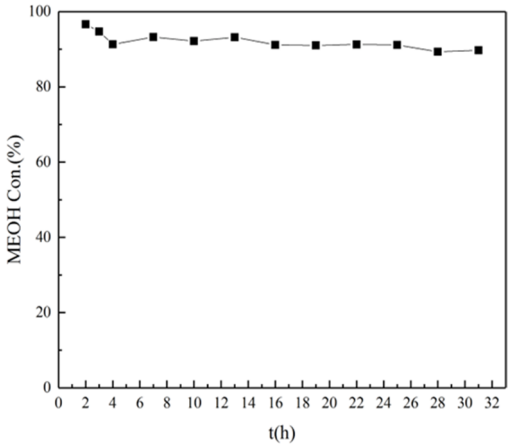


Figure 9. MSR methanol conversion of CuZn catalyst in durability test at 548.15 K.

The power function rate equation is one of the most commonly used phenomenological kinetic models [23]. Its expression form is simple and accurate within the scope of application, and it is generally used to guide industrial production. The methanol steam reforming reaction process includes the MSR main reaction and MD, rWGS, and other side reactions. Under the condition of T $\leq$ 548.15 K, the content of CO produced in this experiment is low. Under the condition of excluding other side reactions, the single-rate PL model of MSR reaction is established, as in Formulas (13) and (14):

$$r_{SR} = k_{SR} exp\left(\frac{-E_a}{RT}\right) P_{CH_3OH}^n P_{H_2O}^m \left(1 - \frac{P_{CO_2} P_{H_2}^3}{K_{SR} P_{CH_3OH} P_{H_2O}}\right) \quad (13)$$

$$k_{SR} = exp\left(-\frac{50240 - 170.98T - 0.0264T^2}{RT}\right) \quad (14)$$

k_{SR} is the pre-exponential factor of the MSR reaction, E_a is the reaction activation energy, R is the general gas constant, T is the reaction temperature, n and m are the partial pressure series of methanol and water, respectively, P_i is the partial pressure of the components, and k_{SR} is the equilibrium constant expressed by pressure. As shown in Formula (15), k_{SR} increases with the increase in temperature, and the equilibrium constant is greater than 10^4 in the temperature range of 508.15 K–548.15 K. Therefore, the single-rate PL model can be simplified as follows:

$$r_{SR} = k_0 exp\left(\frac{-E_a}{RT}\right) P_{CH_3OH}^n P_{H_2O}^m \quad (15)$$

According to the principle of integral reactor [24], the integral form of MSR rate is

$$-r_A dW = F_{A0} dX_A \quad (16)$$

$$\frac{W}{F_{AO}} = \int_O^{AF} \frac{dX_A}{-r_A} \quad (17)$$

F_{A0} is the molar flow rate of methanol, which is the methanol reaction rate per unit mass of catalyst in unit time; W is the mass of catalyst; and X_A is the methanol conversion rate. The relationship between X_A and the partial pressure of each component is shown in Formula (18). The by-product CO concentration is low and can be ignored. So, it can be simplified to Formula (19), and the methanol conversion rate is replaced by the CO_2 generation rate:

$$X_A = \left(P_{CO_2} + P_{CO}\right) / \left(P_{CO_2} + P_{CO} + P_{CH_3OH}\right) \quad (18)$$

$$X_A = P_{CO_2} / \left(P_{CO2} + P_{CH_3OH}\right) = X_{CO_2} \quad (19)$$

The change of CO_2 production rate with W/F is shown in Figure 10. The data are fitted by cubic polynomial regression analysis, and the relationship with W/F can be obtained by derivation:

$$X_A = a\left(\frac{1}{W/F_{AO}}\right) + b\left(\frac{1}{W/F_{AO}}\right)^2 + c\left(\frac{1}{W/F_{AO}}\right)^3 \quad (20)$$

$$r_A = a + 2b\left(\frac{1}{W/F_{AO}}\right) + 3c\left(\frac{1}{W/F_{AO}}\right)^2 \quad (21)$$

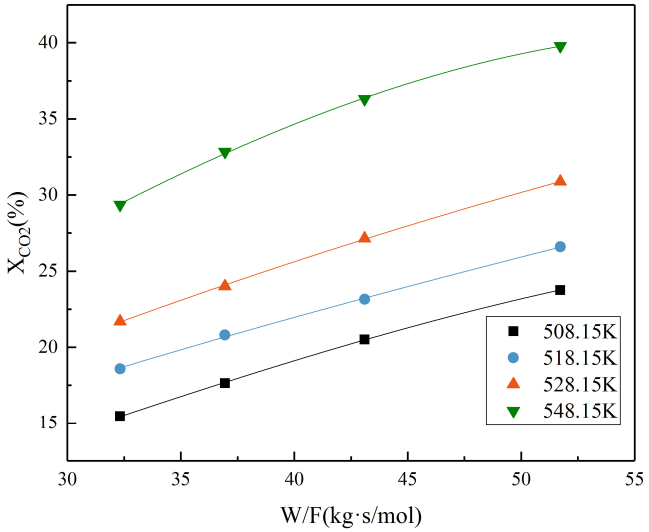


Figure 10. Effects of space velocity on X_{CO2} at different temperatures (W/M = 2, 1 atm).

Two methods are used to solve the problem, which are linearization and direct nonlinear fitting. Through the multiple linear least squares algorithm, the multiple correlation coefficient is less than 0.9, the model is not significant, and the reaction order is obviously unreasonable, being completely divorced from the actual physical significance, so it is not used. The fitting method is to construct the objective function, and the Levenberg–Marquardt algorithm in the nonlinear curve fitting in Origin is used to fit and directly solve the parameter values (Formula (22)):

$$S = \sum_i \left(r_{SR} - \hat{r_{SR}}\right)^2 \quad (22)$$

After nonlinearization, the statistical test results of the kinetic model parameter F are shown in Table 4, ρ^2 is greater than 0.9, and $F_{M,\,N\text{-}M\text{-}1}$ is 206.5, which is more than 10 times greater than $F_{0.05}$ with a confidence region of 95%, indicating that the model equation is significant and credible. The comparison between the calculated value and the experimental value of the reaction rate of the PL model is shown in Figure 11. The fitting effect in the low-reaction-rate section is better than that in the high-reaction-rate section. After removing a significant deviation point, the data points are evenly distributed on both sides of the diagonal line, with an average relative error of 9.95%. The error between the model value and the experimental value is within the acceptable range, and the fitting effect is ideal, which can meet the requirements of the subsequent MSR reaction simulation.

Table 4. Statistical test of PL model parameters after linearization.

N	M	ρ^2	$F_{M,\,N\text{-}M\text{-}1}$	$F_{0.05}$
16	4	0.9361	206.5	1.366×10^{-10}

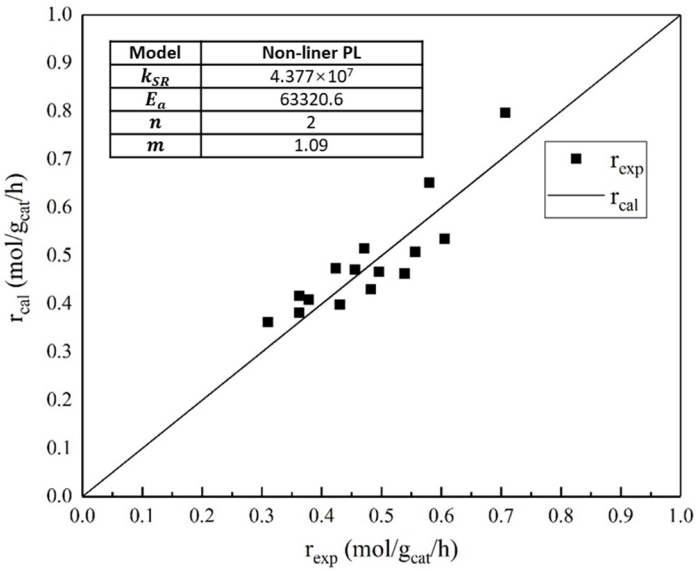


Figure 11. Comparation of calculation and experiment values of reaction rate after linearization.

The final single-rate PL model expression, Formula (23):

$$r_{SR} = 4.377 \times 10^7 \exp\left(\frac{-63320.6}{RT}\right) P_{CH_3OH}^2 P_{H_2O}^{1.09} \quad (23)$$

The kinetic model of the MSR reaction is partially summarized as shown in Supplementary Table S1. It can be seen that the activation energy of MSR is in the range of 76–120 kJ/mol, the activation energy of ME is in the range of 114–168 kJ/mol, and the activation energy of rWGS is in the range of 70–110 kJ/mol [25–28]. The kinetic models of MSR with different catalysts and reactors are different. The activation energy of the MSR reaction obtained in this study is 63.32 kJ/mol, which is lower than that of common statistical catalysts, which explains the high catalytic activity of the CuZn catalyst used in this study.

The MSR reaction is a complex gas–solid phase catalytic process, and there are complex flow, mass, and heat transfer situations in the reformer. The chemical reaction module is used to simulate the catalytic reaction. The catalytic layer is a porous medium layer, the flow adopts the laminar flow module of COMSOL, and the mass transfer module in the porous medium is enabled. The heat transfer involves the heat transfer in the porous medium layer. The porous medium heat transfer module is selected. Considering the excessive air velocity and ignoring the influence of external diffusion, the control equations are as follows:

Flow equation:

$$\frac{1}{\varepsilon_p}\rho(u\cdot\nabla)u\frac{1}{\varepsilon_p} = \nabla\cdot[-pI+K] - \left(\mu\kappa^{-1} + \beta\rho|u| + \frac{Q_m}{\varepsilon_p^2}\right)u + F \quad (24)$$

$$K = \mu\frac{1}{\varepsilon_p}(\nabla u + (\nabla u)^T) - \frac{2}{3}\mu\frac{1}{\varepsilon_p}(\nabla\cdot u)I \quad (25)$$

$$\nabla\cdot(\rho\boldsymbol{u}) = Q_m \quad (26)$$

Heat conduction equation:

$$\rho_f C_{p,f} u\cdot\nabla T + \nabla\cdot q = Q + Q_p + Q_{vd} + Q_{geo} \quad (27)$$

$$q = -k_{eff}\nabla T \quad (28)$$

$$k_{eff} = \theta_s k_s + \varepsilon_p k_f + k_{disp} \tag{29}$$

Diffusion equation:

$$\nabla \cdot j_i + \rho(u \cdot \nabla)\omega_i = R_i \tag{30}$$

$$D_{e,ik} = f_e(\varepsilon_p, \tau_F) D_{ik}, \quad D_{e,i}^T = f_e(\varepsilon_p, \tau_F) D_i^T \tag{31}$$

$$D_i^m = \frac{1-\omega_i}{\sum_{k \neq i} \frac{x_k}{D_{e,ik}}}, \quad M_n = \left(\sum_i \frac{\omega_i}{M_i}\right)^{-1}, \quad j_{c,i} = \rho \omega_i \sum_k \frac{M_i}{M_n} D_k^m \nabla x_k \tag{32}$$

The kinetic equation after unit correction:

$$r_{SR} = 4.377 \times 10^7 exp\left(\frac{-63320.6}{RT}\right) P_{CH_3OH}^2 P_{H_2O}^{1.09} \tag{33}$$

4. Experiment

4.1. Catalyst Preparation

The size of the commercial aluminum mesh is 1.2 × 0.32 mm, the thickness is 0.5 mm, and the mesh shape is rhombus. Prepare 10 wt % NaOH and 10 wt % HNO_3 to pretreat the aluminum mesh to remove surface impurities. The monolithic γ-Al_2O_3/Al carrier was prepared by anodic oxidation method [29,30] referring to the preliminary work of our laboratory. The specific preparation method is shown in Supplementary Materials S1. ZnO/γ-Al_2O_3/Al was prepared by IW impregnation method, in which Zn $(NO_3)_2$ (99%) was heated to liquid state at 90 °C, and then γ-Al_2O_3/Al was completely immersed in liquid Zn $(NO_3)_2$ solution for 1 h. After washing and drying, ZnO/γ-Al_2O_3/Al was calcined at 500 °C or 4 h in a muffle furnace. The CuZn/γ-Al_2O_3/Al was obtained by impregnated in 1.5 mol/L Cu $(NO_3)_2$ solution, controlling the pH value at about 4, taking out after 12 h, and then, the catalyst was washed with deionized water and dried naturally and was finally calcined at 500 °C for 4 h in a muffle furnace.

4.2. Catalyst Evaluation System

The methanol steam reforming (MSR) experiment was carried out in a stainless steel MSR reformer with a diameter of 11 mm. The mesh catalyst (3.0 g), cut by about 20 mesh, and the quartz sand, with a 20–50 mesh, were pre-mixed to a volume of about 7.5 mL and then filled into the reformer. In order to ensure the reliability of the experimental data, repeated tests were performed on the same batch of catalysts to obtain multiple sets of data, and a set of tests was selected to test the durability of the CuZn catalyst at the highest reaction temperature of 548.15 K. Based on this, kinetic experiments were carried out.

The catalyst (1.0 g) was cut into discoidal mesh types of 10 mm and strung together; these catalysts were mesh-aligned and rotated between two adjacent layers to form different stacking forms with a certain angle, as exhibited in Figure 12, and the activity of different forms of catalysts was tested. The evaluation method, the calculation of methanol conversion, H_2 yield, product selectivity, and conversion frequency are introduced in Supplementary Materials S2.

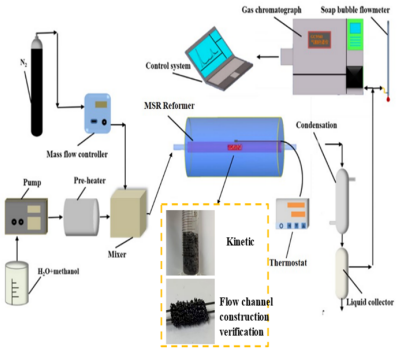


Figure 12. Experimental apparatus for activity and durability testing system in MSR.

5. Conclusions

In this work, a mesh-type structured CuZn-based catalyst prepared by self-growth on an ordered nanoporous carrier γ-Al_2O_3/Al was developed for methanol steam reforming reactions. On this basis, a 3D theoretical model of the MSR reformer was established.

Firstly, the MSR reaction kinetics of the mesh-type structured CuZn catalyst was studied. The PL-type kinetic equation of single rate was selected. On the basis of catalyst stability and elimination of internal and external diffusion, the kinetic equation was obtained by kinetic experiments in the reformer. The results of the nonlinear solution are credible and significant. Considering that the MSR reaction is a complex gas–solid phase catalytic process, there are complex flow, mass, and heat transfers in the reformer. The final unit corrected kinetic equation is as follows:

$$r_{SR} = 4.377 \times 10^7 \exp\left(\frac{-63320.6}{RT}\right) P_{CH_3OH}^2 P_{H_2O}^{1.09}$$

Secondly, based on the characteristics that the network structured catalyst can construct the flow channel through different distribution configurations, a simulation of the structured catalyst in the reforming reactor was carried out, and the influence of the catalyst stacking form and the pore shape on the three-transmission and one-reaction was further analyzed. Finally, the following points were obtained to optimize the catalyst distribution configuration in the reformer to promote mass and heat transfer:

(1) The flow channel constructed by the 'hole-to-edge' configuration of the rhombic structured catalyst was the best, and the highest methanol conversion rate and the highest mass and heat transfer efficiency were obtained, which improved the catalyst and reactor utilization to the greatest extent.

(2) The mesh shape of different catalysts has a significant effect on the reaction. The pressure drop of the circular channel is the smallest, and the mass transfer and heat transfer ability is the strongest. The mixing and uniform distribution of the reactants are promoted by superimposing the turbulence of the channel shape.

The above viewpoints have a certain guiding significance for the application and design of structured catalysts in reforming reactors.

Supplementary Materials: The following supporting information can be downloaded at: https://www.mdpi.com/article/10.3390/catal14120913/s1.

Author Contributions: Conceptualization, methodology, writing—original draft preparation, writing—review and editing Y.X.; software, Y.X. and H.L.; supervision, project administration, funding acquisition, review and editing, Q.Z. All authors have read and agreed to the published version of the manuscript.

Funding: This research was funded by the Fundamental Research Funds for the Central Universities, grant number JKA01241710.

Data Availability Statement: Data are contained within the article and Supplementary Materials.

Conflicts of Interest: The authors declare no conflicts of interest.

References

1. Garcia, G.; Arriola, E.; Chen, W.-H.; De Luna, M.D. A comprehensive review of hydrogen production from methanol thermochemical conversion for sustainability. *Energy* **2021**, *217*, 119384. [CrossRef]
2. Kannah, R.Y.; Kavitha, S.; Preethi; Karthikeyan, O.P.; Kumar, G.; Dai-Viet, N.V.; Banu, J.R. Techno-economic assessment of various hydrogen production methods—A review. *Bioresour. Technol.* **2021**, *319*, 124175.
3. Xu, X.; Zhou, Q.; Yu, D. The future of hydrogen energy: Bio-hydrogen production technology. *Int. J. Hydrogen Energy* **2022**, *47*, 33677–33698. [CrossRef]
4. Hou, J.; Yang, M.; Ke, C.; Wei, G.; Priest, C.; Qiao, Z.; Wu, G.; Zhang, J. Platinum-group-metal catalysts for proton exchange membrane fuel cells: From catalyst design to electrode structure optimization. *EnergyChem* **2020**, *2*, 100023. [CrossRef]
5. Frei, M.S.; Mondelli, C.; Short, M.I.; Pérez-Ramírez, J. Methanol as a Hydrogen Carrier: Kinetic and Thermodynamic Drivers for its CO_2-Based Synthesis and Reforming over Heterogeneous Catalysts. *ChemSusChem* **2020**, *13*, 6330–6337. [CrossRef]

6. Dudukovic, M.P.; Larachi, F.; Mills, P.L. Multiphase catalytic reactors: A perspective on current knowledge and future trends. *Catal. Rev. Sci. Eng.* **2002**, *44*, 123–246. [CrossRef]
7. Achomo, M.A.; Kumar, A.; Peela, N.R.; Muthukumar, P. Hydrogen production from steam reforming of methanol: A comprehensive review on thermodynamics, catalysts, reactors, and kinetic studies. *Int. J. Hydrogen Energy* **2024**, *58*, 1640–1672. [CrossRef]
8. Cao, Z.; Bian, H.; Xie, Z.; Ji, L.; Zhang, Q. Research and improvement on the performance of Ti modified Mn based catalysts for removing ozone at room temp. *J. Guizhou Norm. Coll.* **2024**, *42*, 75–83. (In Chinese)
9. Zhang, G.; Zhao, J.; Yang, T.; Zhang, Q.; Zhang, L. In-situ self-assembled Cu_2O/ZnO core-shell catalysts synergistically enhance the durability of methanol steam reforming. *Appl. Catal. A Gen.* **2021**, *616*, 118072. [CrossRef]
10. Thompson, G.E.; Wood, G.C. Porous anodic film formation on aluminium. *Nature* **1981**, *290*, 230–232. [CrossRef]
11. Kameyama, H. Heat Transfer Material with Porous Alumina Layer. *Suiso Energy Shisutemu* **1995**, *20*.
12. Stankiewicz, A. Process intensification in in-line monolithic reactor. *Chem. Eng. Sci.* **2001**, *56*, 359–364. [CrossRef]
13. Heck, M.R.; Gulati, S.; Farrauto, J.R. The application of monoliths for gas phase catalytic reactions. *Chem. Eng. J.* **2001**, *82*, 149–156. [CrossRef]
14. Groppi, G.; Tronconi, E. Honeycomb Supports with High Thermal Conductivity for Gas/Solid Chemical Processes. *Catal. Today* **2005**, *105*, 297–304. [CrossRef]
15. Sidhu, T.P.; Govil, A.; Roy, S. Optimal monolithic configuration for heat integrated ethanol steam reformer. *Int. J. Hydrogen Energy* **2017**, *42*, 7770–7785. [CrossRef]
16. Qian, S.; Liu, H.; Wang, Y.; Mei, D. Structural optimization of 3D printed SiC scaffold with gradient pore size distribution as catalyst support for methanol steam reforming. *Fuel* **2023**, *341*, 127612. [CrossRef]
17. Ramanathan, K.; Balakotaiah, V.; West, H.D. Geometry effects on ignition in catalytic monoliths. *AIChE J.* **2004**, *50*, 1493–1509. [CrossRef]
18. Erdinç, E.; Caglayan, S.B.; Aksoylu, E.A. Methane OSR over Pt-Ni/δ-Al_2O_3: Performance and power law type kinetics. *Int. J. Hydrogen Energy* **2017**, *42*, 20568–20578. [CrossRef]
19. El-Shafie, M.; Harada, H.; Yajima, T.; Tsuda, S.; Inazu, K.; Kawajiri, Y. A comprehensive analysis of ammonia synthesis over a commercial iron-based catalyst using differential and integral reactor models. *Int. J. Hydrogen Energy* **2024**, *58*, 1009–1019. [CrossRef]
20. Patel, S.; Pant, K.K. Experimental study and mechanistic kinetic modeling for selective production of hydro-gen via catalytic steam reforming of methanol. *Chem. Eng. Sci.* **2007**, *62*, 5425–5435. [CrossRef]
21. Purnama, H.; Ressler, T.; Jentoft, R.; Soerijanto, H.; Schlögl, R.; Schomäcker, R. CO formation/selectivity for steam reforming of methanol with a commercial CuO/ZnO/Al_2O_3 catalyst. *Appl. Catal. A Gen.* **2004**, *259*, 83–94. [CrossRef]
22. Sá, S.; Sousa, J.M.; Mendes, A. Steam reforming of methanol over a CuO/ZnO/Al_2O_3 catalyst, part I: Kinetic modelling. *Chem. Eng. Sci.* **2011**, *66*, 4913–4921. [CrossRef]
23. Wan, Y.; Zhou, Z.; Cheng, Z. Hydrogen production from steam reforming of methanol over CuO/ZnO/Al_2O_3 catalysts: Catalytic performance and kinetic modeling. *Chin. J. Chem. Eng.* **2016**, *24*, 1186–1194. [CrossRef]
24. Wang, Q.; Zhang, G.; Zhao, J.; Zhang, L. Robust Mesh-type structured CuFeMg/γ-Al_2O_3/Al catalyst for methanol steam reforming in microreactors. *Int. J. Hydrogen Energy* **2022**, *47*, 25256–25265. [CrossRef]
25. Zhang, G.; Zhao, J.; Wang, Q.; Yang, T.; Zhang, Q.; Zhang, L. FFast start-up structured CuFeMg/Al_2O_3 catalyst applied in microreactor for efficient hydrogen production in methanol steam reforming. *Chem. Eng. J.* **2021**, *426*, 130644. [CrossRef]
26. Li, X.; Wang, Y.; Li, L.; Zhang, R.; Ren, H.; Li, W.; Tang, Z.; Zhang, D. Research progress on simulation of multiscale mass transfer processes in gas-solid system by computational mass transfer. *Particuology* **2024**, *90*, 478–492. [CrossRef]
27. Skrzypacz, P.; Chalkarova, N.; Golman, B.; Andreev, V.; Schieweck, F. Numerical simulations of dead zone formation in the catalytic flow-through membrane reactor. *Comput. Chem. Eng.* **2021**, *152*, 107368. [CrossRef]
28. Cui, X.; Kær, K.S. Two-dimensional thermal analysis of radial heat transfer of monoliths in small-scale steam methane reforming. *Int. J. Hydrogen Energy* **2018**, *43*, 11952–11968. [CrossRef]
29. Palma, V.; Martino, M.; Meloni, E.; Ricca, A. Novel structured catalysts configuration for intensification of steam reforming of methane. *Int. J. Hydrogen Energy* **2017**, *42*, 1629–1638. [CrossRef]
30. Vennela, N.; Mondal, S.; De, S.; Bhattacharjee, S. Sherwood number in flow through parallel porous plates (Microchannel) due to pressure and electroosmotic flow. *AIChE J.* **2012**, *58*, 1693–1703. [CrossRef]

Disclaimer/Publisher's Note: The statements, opinions and data contained in all publications are solely those of the individual author(s) and contributor(s) and not of MDPI and/or the editor(s). MDPI and/or the editor(s) disclaim responsibility for any injury to people or property resulting from any ideas, methods, instructions or products referred to in the content.